

Synthesis_of_highly_self_dual_ doped_O_P_carbon_nanoshee ts_derived

by Rika Taslim

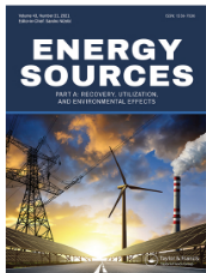
Submission date: 10-Jul-2023 08:46PM (UTC+0700)

Submission ID: 2129130727

File name: esis_of_highly_self_dual_doped_O_P_carbon_nanosheets_derived.pdf (3M)

Word count: 7975

Character count: 44484



Synthesis of highly self-dual-doped O, P carbon nanosheets derived from banana stem fiber for high-performance supercapacitor electrode

Erman Taer, Novi Yanti, Dinda Putri Azaria, Apriwandi Apriwandi, Rika Taslim & Dahyunir Dahlan

To cite this article: Erman Taer, Novi Yanti, Dinda Putri Azaria, Apriwandi Apriwandi, Rika Taslim & Dahyunir Dahlan (2023) Synthesis of highly self-dual-doped O, P carbon nanosheets derived from banana stem fiber for high-performance supercapacitor electrode, Energy Sources, Part A: Recovery, Utilization, and Environmental Effects, 45:3, 9217-9230, DOI: [10.1080/15567036.2023.2233448](https://doi.org/10.1080/15567036.2023.2233448)

To link to this article: <https://doi.org/10.1080/15567036.2023.2233448>



Published online: 09 Jul 2023.



Submit your article to this journal [↗](#)







View related articles [↗](#)



View Crossmark data [↗](#)



Synthesis of highly self-dual-doped O, P carbon nanosheets derived from banana stem fiber for high-performance supercapacitor electrode

Erman Taer ^a, Novi Yanti ^a, Dinda Putri Azaria^a, Apriwandi Apriwandi ^a, Rika Taslim ^b, and Dahyunir Dahlan^c

^aDepartment of Physics, University of Riau, Simpang Baru, Riau, Indonesia; ^bDepartment of Industrial Engineering, State Islamic University of Sultan Syarif Kasim, Simpang Baru, Riau, Indonesia; ^cDepartment of Physics, University of Andalas, Padang, West Sumatra, Indonesia

ABSTRACT

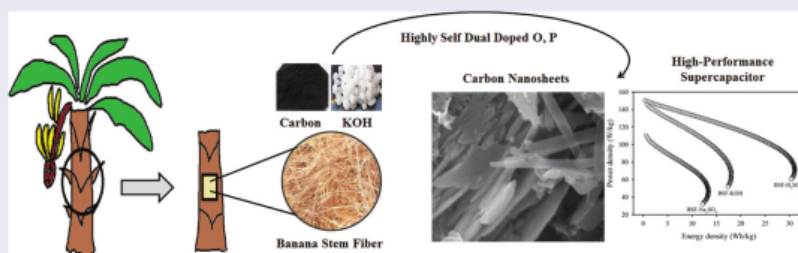
In the present study, the development of a supercapacitor electrode using activated carbon (AC) derived from natural banana stem fiber (BSF) was presented. To enhance AC-BSF performance, nanosheets with favorable pore structures were incorporated, enriched with O and P doping. The production process involved crushing and heating BSF particles at high temperatures, with the addition of 0.5 M KOH as a reaction agent and developer of porous carbon structures with high density. The physical properties of AC-BSF were determined through density calculations, which revealed a shrinkage up to 34%. The material exhibited amorphous properties characterized by gentle peaks at diffraction angles (2θ) of 23.06–25.01° and 44.63–46.07°. The wettability of AC-BSF was attributed to the presence of O-H functional groups, micro-mesopores structure was confirmed by the type IV isotherm curve. AC-BSF- H_2SO_4 showed the highest specific capacitance value of 206.76 F/g. The increase in the performance of the AC-BSF electrode could primarily be attributed to its dual doping with O (24.15%) and P (4.37%) as well as the contribution of pseudocapacitance. These findings show the significant potential of O and P-doped multi-heteroatom carbon nanosheets derived from banana stem fibers in advancing new strategies for the development of high-energy-density and high-power supercapacitor materials.

ARTICLE HISTORY

Received 1 June 2023
Revised 28 June 2023
Accepted 29 June 2023



KEYWORDS

Banana_stem_fibre;
carbon_electrode;
nanosheet; self_dual_doped;
supercapacitors



Introduction

The growth in human population and socioeconomic activities has led to an increased demand for energy, particularly electricity (Yan et al. 2023). However, the utilization of nonrenewable energy sources such as fossil fuels (coal, oil, and natural gas) is highly inefficient in the long run

CONTACT Erman Taer  erman.taer@lecturer.unri.ac.id; erman_taer@yahoo.com  Department of Physics, University of Riau, Simpang Baru, Riau 28293, Indonesia

© 2023 Taylor & Francis Group, LLC

and poses significant environmental problems (Mangisetti, Kamaraj, and Sundara 2021). The long-term exploitation of these nonrenewable sources contributes to global climate change, loss of biodiversity, air and water pollution, and rising sea levels. As a result, there is a growing need for innovative ideas to explore abundant, sustainable, and renewable energy resources, such as solar, water, and wind power (Lesbayev et al. 2023; Malhotra, Valiollahi, and Wiinikka 2023). These energy sources have limitations for long-term use due to their regional and unstable nature. Therefore, it is necessary to innovate the development of energy storage devices that are sustainable, environmentally friendly, and cost-effective. Nanogenerator and supercapacitor technologies are considered as promising technologies in ensuring world energy sustainability (Wang et al. 2022, 2023; Zhang et al. 2023). Supercapacitors have garnered considerable attention as energy storage devices due to their ability to deliver high power density, low maintenance costs and high reliability with long storage cycles (Priya, Kennedy, and Anand 2023; Zhou and Yao 2022). They store energy through electrostatic forces, facilitating charge transfer at the interface between the electrode/electrolyte without involving faradaic reactions that produce an electrochemical double layer (Dong et al. 2023; Fang et al. 2022). This characteristic makes an electric double-layer capacitor (EDLC) a promising type of supercapacitor with stable and long-lasting charge capabilities (Shaku et al. 2023; Taer et al. 2022). Moreover, supercapacitors that employ pseudocapacitance mechanisms can increase the specific capacitance and energy density by utilizing redox processes involving doping elements such as O, N, P, Zn, Cl, B, Xe, etc (Liu et al. 2023; Yang et al. 2023). The applications of supercapacitors have been explored in various fields, including hybrid electric vehicles, electronic devices, and high-power-demanding machinery such as drilling machines. However, the application of supercapacitors consisting of 4 main components, namely electrodes, current collectors, separators, and electrolytes as commercial-based energy storage devices are hindered by their low energy density, which remains a challenge.

The current focus in the development of supercapacitors is to increase the energy density while maintaining the power density and specific capacitance. Achieving this goal involves selecting the appropriate electrode material, such as carbon-based nanomaterials such as graphene, carbon aerogel, carbon nanotubes, carbon nanofibers, etc (Li et al. 2021), metal oxide such as MnO, SiO₂, ZnO, and polymer conducting such as PAN, or PaNI. Carbon nanofiber possess an interesting characteristic, for example, their natural fiber structure is interconnected, which reduces charging distance, increase charge transfer efficiency, and lower carbon electrode resistance (Taer et al. 2022). In addition, the addition of the Faraday reaction through heteroatom doping is an effective choice to improve the performance of supercapacitors. As reported by (Fu et al. 2020) demonstrated carbon nanofibers based on a mixture of metal oxides and carbon-based graphene. They produced a carbon nanofiber-based electrode material with a specific capacitance of 334 F/g. Furthermore (Shang et al. 2021), synthesizing carbon nanofibers with chitin and co-doped nitrogen has confirmed the amazing electrochemical properties of supercapacitors. The flexibility of the conductive nanofiber coupled with the wettability and redox reaction of the N-doped produces a high specific capacitance of 182 F/g on the two-electrode system. On the other hand, biomass-based carbon nanofiber has been studied by (Farma et al. 2021) from bamboo stem waste. Significantly they produced dense nanofiber structures with capacitive properties of 174 F/g.

Carbon nanofibers-nanosheet, as one-two dimensional carbon materials, possess a large surface area and high electronic conductivity (Chen et al. 2022). They exhibit excellent absorption power with micropores dominating their pore sizes. The structural units of nanofibers display a hexagonal arrangement similar to graphite (Shaku et al. 2023). The interconnected structures within carbon nanofibers facilitate the transfer of ions within the carbon matrix, thereby supporting the performance of the electrodes in supercapacitor cells (Taer et al. 2023).

However, most of the above studies used complex synthetic approaches to obtain nanofiber structures such as using complex electrospinning, adding expensive PAN or PANI materials, and adding corrosive and toxic metal oxide materials. Although several reports state that nanofiber structures can be synthesized from natural biomass materials, not all biomass has this potential and

requires additional external doping to maintain their wettability. Therefore, information is urgently needed on potential origin materials for nanofiber structures that are environmentally friendly and have a promising source of self-doped heteroatom.

Meanwhile, considering the potential of bananas as a crop, with global production reaching 120 million tonnes/year, it is worth noting that Indonesia produced approximately 8.74 million tons in 2021, and this number continues to rise due to high consumer demand (Misran et al. 2022). A banana plant consists of roots, stems, leaves, fruit, and a banana heart. Bananas can be consumed directly or processed in various ways, and their leaves are commonly used as traditional food wrappers. The blossoms are processed into vegetables, while banana stems are usually left to decompose, which can contribute to environmental pollution. Banana stems contain a collection of fibers with high lignin (27.8%), cellulose (43.3%), and hemicellulose (20.6%) contents, making them suitable as carbon sources (Taer et al. 2020). To optimize banana stem fibers as supercapacitor electrode materials, which are believed to influence the ion diffusion process and enhance capacitive properties, several important steps are followed: chemical activation, carbonization, and physical activation.

In this work, we prepared a novel AC-BSF supercapacitor electrode with a 1D-2D nanofiber - nanosheet structure through optimization of natural fibers with novel strategy of KOH chemical activation and one-step integrated pyrolysis. Banana stem fiber was selected as potential biomass to obtain high-quality 1D-2D nanostructure as electrodes. Nanoporous carbon was synthesized through the combined chemical activation of KOH in 0.5 mmol/L solution and integrated one-step pyrolysis in an N_2 & CO_2 gaseous environment. Furthermore, the carbon material is prepared through the latest design with a solid coin-like shape made of a binder that maintains high conductivity. The porous structure of the nanosheet on the AC-BSF electrode is scattered randomly on the surface of the electrode doped with oxygen and phosphorus multi-heteroatoms. The tight bonds between oxygen and nitrogen atoms in the carbon matrix form a stable conductive 2D network structure. This 2D nanosheet structure on AC-BSF promotes charge transfer by shortening ion transport paths which significantly improves electrochemical performance. Wherein, the reactive nonmetals O and P increase the apparent capacitance of the carbon material, thereby increasing the specific capacitance. The AC-BSF- H_2SO_4 electrode simultaneously achieves an extraordinary specific capacitance of 202 F/g at 1 A. In addition, the AC-BSF- H_2SO_4 electrode as a symmetrical electrode of a supercapacitor cell with a nanofiber pore structure produces a high energy density of 31.13 Wh/kg 150.31 W/kg. To the best of our knowledge, no reports are available on the optimization of banana stem fiber as a biomass precursor for the synthesis of multi-heteroatom (O and P) co-doped nanosheet activated carbon using a self-doping strategy via one-step integrated pyrolysis and the influence of an aqueous electrolyte of 1 M H_2SO_4 . Therefore, this study is expected to provide theoretical support for the use of porous carbon 2D nanosheets biomass-based with O, P self-doped as electrode material sources for sustainability supercapacitors.

Experimental section

Materials and chemicals

Banana stem fiber (BSF) was obtained from banana garden waste in Riau, Indonesia. Potassium hydroxide (KOH), Sodium Sulfate (Na_2SO_4), and pH indicator strips (non-bleeding) were purchased from EMSURE Merck KgaA, a chemical reagent company based in Darmstadt, Germany. Sulfuric acid (H_2SO_4) was purchased from Panreac Quimica Sau in Barcelona, part of the European Union. Nitrogen (N_2) inert gas and carbon dioxide (CO_2) reactive gas were purchased from PT. Samator group in Indonesia. Aquades with a pH value of 7 were produced in the chemical engineering laboratory at Riau University.

BSF manufacture

The sample consisted of banana stem fiber waste resulting from logging during the harvesting process. The first step involved peeling the outer skin of the banana stem to efficiently extract the fiber using

the mechanical shaving method. Second, the BSF obtained was washed with running water. Third, the sample was cut into 3–5 cm sizes, and in the fourth, it was dried in the sun for 3 days to reduce humidity and water content, leading to a mass loss of <6%, which served as a characterization parameter.

Preparation of activated carbon

The conversion of BSF to AC-BSF began with a pre-carbonization process using a vacuum electric oven at 50–250°C for 2.5 hours. This process changes the physical condition of the sample, making it brittle and giving it a blackish-brown color (carbon form). The carbon samples were then refined to achieve a micrometer-scale particle size through a crushing process using a mortar and grinding using a ball-milling. The resulting carbon sample was sieved using a 250 mesh sieve to obtain uniform particles <60 µm. This study focused on investigating how the chemical activator, KOH, influenced the physical and electrochemical properties of carbon samples derived from BSF biomass waste. The samples were chemically activated using a thermo scientific hot plate stirrer at a constant temperature and stirring speed (80°C/300 rpm). The chemical activation process involved creating a 0.5 M KOH solution by dissolving 4.2 g KOH in 150 ml of distilled water and stirring for 1 hour. Subsequently, 30 g of BSF carbon was added to the 0.5 M KOH solution and stirred for 2 hours. The KOH-activated BSF carbon samples were dried using an electric oven at 110°C for 1 day to remove any remaining water content from the chemical activation process. The KOH-activated BSF carbon powder samples were converted into monolithic coins through a printing process using a hydraulic press with a pressure of 8 metric tons and a holding time of 2 minutes. AC-BSF with a nanosheet pore structure rich in self-dual doped O, P was produced through a one-stage integrated pyrolysis process (N₂/CO₂) at high temperature using a pantech furnace. Carbonization was carried out in an inert gas environment (N₂) within a temperature range of 30–600°C, with a dwell time of 1 hour. This process aimed to eliminate volatile compounds present in the carbon matrix and achieve a high carbon content. Subsequently, physical activation was performed using a reactive gas (CO₂) at temperatures ranging from 600–850°C, with a holding time of 2.5 hours. This step was employed to enhance the pore structure, increase pore size, and create new pores within the carbon matrix. Finally, the AC-BSF sample was neutralized through a periodic washing process using 1000 ml of distilled water, producing a neutral pH (pH = 7). This procedure was conducted to characterize the physical and electrochemical properties of the sample.

Characterization of physical properties

The of the BSF sample was conducted using thermogravimetric analysis (TGA) with a Shimadzu TGA-50. These measurements served as the fundamental characterizations for this study. The formation and development of the AC-BSF pore structure were predicted based on the theory of decreasing density, which involved the shrinkage of mass, diameter, and thickness of monolithic carbon coins during the N₂/CO₂ pyrolysis process at high temperatures. To analyze the functional groups and wettability of carbon materials, a Fourier-transform infrared (FT-IR) spectroscope was performed using a Shimadzu Prestige 21 Nicolet Avatar 360 IR spectroscope. The crystallographic characteristics of the activated carbon material were determined ⁴² using X-ray diffraction (XRD) with a PANalytical PW3040/60 XRD XPERT PRO instrument. The specific surface area and pore size distribution were evaluated by measuring the amo³⁷ of nitrogen gas absorbed using the Quantachrome Touchwin V1.22 instrument, employing the Brunauer-Emmett-Teller (BET) method and the Barrett-Joyner-Halenda (BJH) equation. The morphological structure of activated carbon coins was examined through scanning electron microscopy (SEM) with a ZEISS EVO 10 vacuum instrument.

Electrochemical characterization

Electrochemical evaluation of AC-BSF was performed in a symmetrical 2-electrode system using a 1 M aqueous electrolyte solution (H_2SO_4 , KOH, and Na_2SO_4). The effect of self-doped dual O and P on the electrochemical performance of nanosheet-activated carbon was determined through cyclic voltammetry (CV) and galvanostatic charge-discharge (GCD) tests. The CV characterization was conducted using the CV UR Rad-Er 5841 Software Cyclic Voltammetry CV V6, while GCD measurements were carried out using the UR Rad-ER 2018 CD instrument. Both the CV and GCD instruments were calibrated with VersaStat II Princeton Applied Research, with an error margin of $\pm 6.0\%$.

Results and discussion

The thermal gravimetric characteristics of BSF carbon were analyzed based on the Thermogravimetric (TG) and Differential Thermal Gravimetry (DTG) curves. The TG curve showed a decrease in carbon mass as the temperature increased, indicating the evaporation of volatile compounds (Choi, Lee, and Jeong 2023). Figure 1a showed the TG curve, which exhibited three stages of mass decomposition attributed to the evaporation of water, moisture, and complex compounds (hemicellulose, cellulose, and lignin), with a maximum decomposition of approximately 41.5% (Kumar et al. 2020; Ye et al. 2020). Similarly, the DTG curve shown in Figure 1b showed three stages of evaporation, confirming the degradation and evaporation of water, hemicellulose, cellulose, and lignin. These results closely aligned with the temperature resistance observed in other biomass materials, such as peanut shells (Açıklan 2021) and *Laurus nobilis* plant (Taer et al. 2023).

Density characterization served as the initial analysis to evaluate the physical properties of AC-BSF concerning the shrinkage of the mass, diameter, and thickness of the carbon monolith after the pyrolysis process. This shrinkage occurred due to the evaporation of non-carbon volatile compounds, as observed in thermal analysis. The evaporation of non-carbon elements indicated the formation of space, leading to a porous structure that served as a storage medium at the electrode. According to Figure 1c, the mass of BSF carbon coins significantly decreased after going through the pyrolysis process. This reduction was attributed to the evaporation of volatile compounds present in the biomass as the temperature rose (Yetri et al. 2020). The drastic decrease in mass led to a stronger arrangement of carbon bonds, as non-carbon elements had evaporated. The density of BSF coins before pyrolysis was measured at 0.91 g/cm^3 , which decreased to 0.62 g/cm^3 after pyrolysis, facilitated by a chemical activator, namely 0.5 M KOH. The reaction between KOH and carbon releases K bonds, resulting in the formation of new compounds, such as K_2CO_3 and H_2O . The K bonds played a crucial role in the formation of micropores. The water vapor formed during the pyrolysis process subsequently evaporated, leaving empty spaces. This pore structure reduced the dimensions of the carbon electrode, which impacted the magnitude of the density reduction.

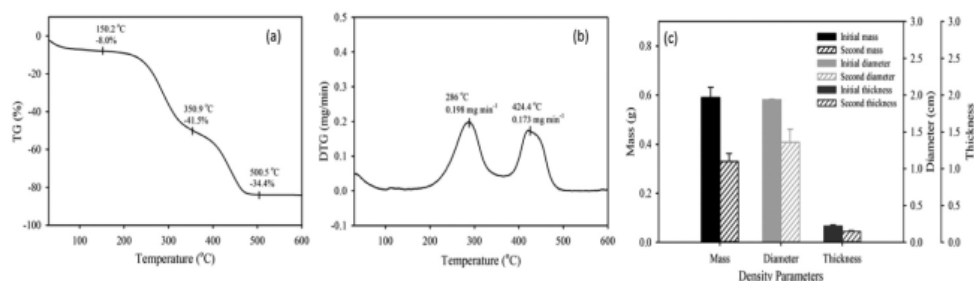


Figure 1. (a) Thermogravimetry (TG) profile, (b) Derivative Thermogravimetry (DTG) profile, and (c) reduction of mass, diameter, and thickness of BSF samples.

FTIR measurements were conducted to further investigate the chemical identity and wettability properties of AC-BSF based on the availability of functional groups, which were influenced by wave number ($1/\text{cm}$) and transmittance (%). As shown in Figure 2a, the peaks at $3925.31\ 1/\text{cm}$ and $3584.20\ 1/\text{cm}$ corresponded to stretching vibrations associated with the O-H functional group. The transmittance reached an absorbance of 17.27%, indicating the presence of carboxylic acid, alcohol, phenol, and hydroxyl group compounds derived from biomass components such as cellulose, hemicellulose, and lignin. This O-H functional group contributed to increased wettability and hydrophilicity, supporting the performance of the electrode in ion absorption (Yaglikci et al. 2020; M.; Zhang et al. 2021). High wettability optimized charge storage and increased super capacitance capacity. Furthermore, the absorption peak at $2917.74\ 1/\text{cm}$ characterized the methyl functional group (C-H) commonly found in hydrocarbon compounds. The strain vibration of the $\text{C}\equiv\text{C}$ functional group at wave numbers ($2377.4, 2298.61, 2235.01, 2169.83,$ and $2111.49\ 1/\text{cm}$) indicated the presence of pure carbon in AC-BSF. The $\text{C}=\text{O}$ strain vibration of the carboxyl and ester functional groups at wave numbers ($1913.27, 1858.34,$ and $1771.79\ 1/\text{cm}$) was attributed to the presence of hemicellulose and lignin in the biomass. The strain vibrations at 1418.07 and $1188.03\ 1/\text{cm}$ were associated with the C-C strain of the phenol group, while the strain at $583.39\ 1/\text{cm}$ was caused by C-O-H. The FTIR spectrum obtained was similar to that of other biomass materials, such as starfruit leaves and mango kernels.

The microstructure and crystallinity levels of the AC-BSF samples were confirmed by X-ray diffraction (XRD). As previously reported, the XRD characterization showed two sloping and several sharp peaks in the diffraction angle range of $10\text{--}60^\circ$, indicating the semi-crystalline nature of the amorphous carbon material as shown in Figure 2b. The physical carbonization-activation process of BSF carbon, which was rich in natural doping of O and P, produced two gently sloping peaks in planes 002 and 100 ($23.06^\circ\text{--}25.01^\circ$ and $43.63^\circ\text{--}45.07^\circ$), indicating low crystallinity due to the formation of

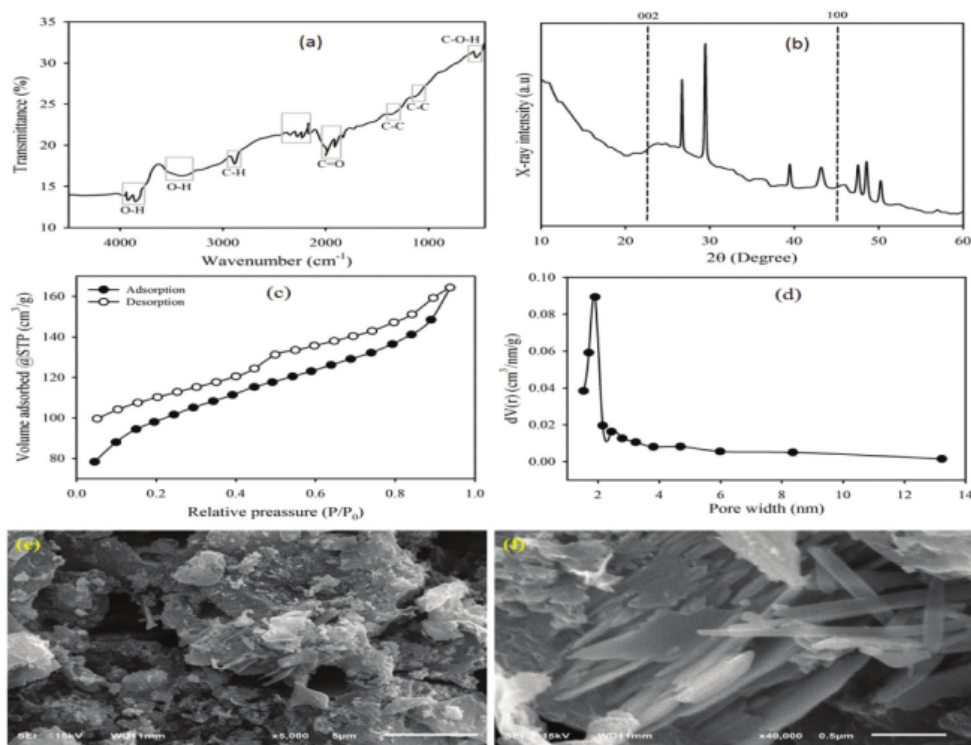


Figure 2. (a) FTIR spectrum, (b) XRD pattern, (c) absorption-desorption N_2 isotherm, (d) pore size distribution, and morphological structure (e) $5000\times$, (f) $40000\times$ of AC-BSF.

a turbo static carbon structure. Plane 002 confirmed the presence of amorphous carbon with a disturbed structure in the biomass-based material, while plane 100 confirmed a graphite-like carbon structure (Awitdrus et al. 2022). The broad diffraction peaks further confirmed the presence of amorphous carbon resembling nanosheets. Additionally, several sharp peaks at angles 26.70°, 29.43°, 39.44°, 43.16°, 47.53°, 48.51°, 50.18° and 56.86°, confirmed the presence of volatile compounds in small quantities. The non-carbon compounds found in biomass materials included K_2CO_3 , SiO_2 , and $CaCO_3$. Specifically, K_2CO_3 was observed at angles of 26.70° and 50.18°, SiO_2 at 29.43° and 56.86° (JCPDS No. 89–1668), as well as $CaCO_3$ at angles of 39.44°, 43.16°, 47.53° and 48.51° (JCPDS No. 82–1690). In general, these crystal substances can adversely affect the capacitive behavior of the electrodes. Crystalline substances can inhibit the growth of carbon porosity and their presence interferes with the insertion-deinsertion of ions at the electrode/electrolyte interface. This phenomenon tends to reduce the capacitance of supercapacitor cells. However, this crystalline substance in the form of an oxide has a positive side in supercapacitor performance. The crystalline oxide substance containing the oxygen element attached to the carbon chain is closely related to the increase in the material's wettability, due to a self-doping effect in the electrode material. A similar analysis was also revealed in previous studies. Notably, these heteroatoms contributed to providing wettability, pseudocapacitance effect, and increased capacitance of the electrode.

The XRD parameters of the AC-BSF electrodes were shown in Table I, with the values of d_{002} and d_{100} being 3.85 Å and 2.02 Å, respectively. These values were typically for biomass-based amorphous carbon materials. The value of d_{002} , which was greater than the graphite value of 0.33 nm, confirmed a well-formed amorphous carbon structure, while the value of d_{100} indicated a weak graphite structure, considered normal for biomass-based activated carbon (Zhang et al. 2021). Furthermore, the height value of the microcrystalline layer (L_c), which was smaller than the width of the microcrystalline layer (L_a) at 6.46 Å and 21.67 Å, respectively, could affect the specific surface area, influencing the specific capacitance value.

Nitrogen adsorption/desorption isotherms were used for BET and BJH analysis to determine the porosity and surface area of AC-BSF at 77 K (Shanmuga Priya, Divya, and Rajalakshmi 2020), as shown in Figure 2c. The isotherms exhibited characteristic adsorption-desorption curves of type IV with H4 hysteresis loops, confirming a multi-scale (micro-meso-macro) porous structure in AC-BSF. Specifically, AC-BSF showed a significant increase in the low-pressure range ($P/P_0 < 0.3$), indicating the dominance of a microporous structure (Kigozi et al. 2023). In the medium-high relative pressure region ($0.4 < P/P_0 < 0.91$), an open hysteresis loop revealed the presence of mesopores. Moreover, absorption at relatively high pressure ($P/P_0 > 0.91$) confirmed the existence of macro pores in the sample. Figure 2d showed the pore distribution on the surface of the AC-BSF electrode. The availability of micropores was confirmed by the high pore volume ranging from 0.04 to 0.09 $cm^3/nm/g$, as well as the BJH measurement data, which indicated a micropore surface area of up to 182.04 m^2/g . Furthermore, the hysteresis loop verified a mesoporous surface area of 144.31 m^2/g . The formation of micropores could be attributed to the use of chemical activators and the reaction between carbon and potassium carbonate (KOH), which generated K bonds and created a microporous structure in the activated carbon material. The presence of micro-meso pores in AC-BSF played a crucial role as active sites, enhancing the performance of supercapacitor electrodes. Micropores contributed to increased energy density, while mesopores facilitated increased power density by enabling smooth ion transport (Xuan et al. 2023). Based on nitrogen adsorption/desorption data, the specific surface area of AC-BSF reached 326.35 m^2/g , and its appropriate porosity between the electrodes supported the achievement of high specific capacitance in supercapacitors.

Unique combinations of pore structures, including sheets and fibers, were observed on the surface of the AC-BSF electrode using a Scanning Electron Microscope (SEM) at 5000× and 40,000× magnification as shown in Figure 2(e,f). The initial structure of the biomass, the chemical activating agent, and the integrated pyrolysis of high-temperature physical activation-carbonization were identified as significant factors in modifying the morphology and developing the pore structure of the AC-BSF samples. The evaporation of volatile compounds, such as cellulose and lignin, was confirmed to have generated porous structures with fiber- and sheet-like morphology, influenced by the pyrolysis route and KOH activation. In Figure 2f, a sheet structure with a diameter of 0.56 nm to 1.97 μm was

observed, decorated with a porous fiber structure ranging from 31 nm to 109 nm. The addition of a KOH activator and physical activation at a temperature of 850°C increased the number of reactions with the BSF carbon matrix, promoting higher activation efficiency and leading to the formation of a porous sheet structure. The nanofiber pore structure provided larger pore sizes, facilitating the formation of electrolyte ion pairs and ensuring smooth charge transport between the pores. This combination of fiber and sheet morphology was ideal for enhancing the conductivity of supercapacitor cell electrodes. The sheet structure in AC-BSF provided numerous available active sites, enabling the generation of additional pairs of charges to form an electric double layer, as well as facilitating smooth ion access to fill the electrode pores (Wang et al. 2021). The interconnected fiber structure shortened ion transport routes, leading to increased energy. It was crucial to select biomass with superior characteristics, such as banana stem fiber rich in cellulose and lignin, as it served as a configuration of nanosheet material that enhanced the conductivity of carbon electrode materials suitable for supercapacitor energy storage applications.

Integrated pyrolysis (N_2/CO_2) and KOH chemical activation successfully optimized the production of high-purity activated carbon, as confirmed by the analysis of the chemical composition using Energy Dispersive Spectroscopy (EDS) as seen in Table 1. AC-BSF exhibited a carbon element percentage of 69.56%, supporting the amorphous porosity of the sample. Oxygen was identified as the second dominant element, accounting for 22.42% of the composition. The presence of oxygen in this activated carbon material contributed to increased hydrophobicity, facilitating the absorption of molecular ions from the decomposed electrolyte. In addition, elemental oxygen could act as a heteroatom doping agent, producing apparent capacitance and increased specific capacitance (Taer et al. 2020). The presence of elemental phosphorus at 2.09% in the form of PC bonds allegedly contributed to the improved electrochemical performance of AC-BSF as a heteroatom doping agent. The suitable amount of phosphorus atom in the carbon matrix was known to increase amorphous porosity and provide more active sites in the electrochemical double layer. Moreover, the detection of other non-carbon elements such as Ca, Si, and Mg was attributed to the natural elements comprising the biomass of banana stem fiber.

The electrochemical properties of the AC BSF electrode were evaluated through cyclic voltammetry (CV) measurements using the Physics CV UR Rad-ER 5481 tool, within a low potential window (0–1) V and a scan rate of 1, 2, and 5 mV/s (Figure 3a–c). This test was conducted with different types of acidic, basic, and neutral 1 M aqueous electrolytes (H_2SO_4 , KOH, and Na_2SO_4). The output of the CV measurement exhibited a distorted rectangular curve, depicting the relationship between current and voltage density. This characteristic shape is commonly observed in supercapacitor carbon electrodes derived from biomass. The BSF- H_2SO_4 AC electrode demonstrated a wider curve with a slight hump, resulting from the presence of O and P heteroatoms attached to the carbon chain, acting as self-doping agents that produced oxidation-reduction reactions during the electrochemical process. This redox reaction contributed to a pseudocapacitance effect, characterized by a sudden increase in current, leading to a wider curve with slight hump-like bumps, which confirmed a higher specific capacitance.

In general, the type of electrolytes used in supercapacitors significantly impacted their electrochemical performance due to differences in ionic radius, ionic conductivity, and ionic mobility. The H^+ ions found in the H_2SO_4 electrolyte solution possessed a smaller ionic radius compared to K^+ in the KOH electrolyte and Na^+ in the Na_2SO_4 electrolyte. Specifically, the ionic radius of H^+ is 0.28 nm, while K^+ and Na^+ had larger ionic radii, measuring 0.31 nm and 0.35 nm, respectively. The smaller ionic radius of H^+ allowed for easier filling of electrode pores. Furthermore, the H_2SO_4 electrolyte

Table 1. A) interlayer spacing (d_{002} and d_{100}), microcrystallin dimension (L_c and L_a), and chemical status of AC-BSF.

hkl field	θ (°)	2θ (°)	d_{002} (Å)	d_{100} (Å)	L_c (Å)	L_a (Å)	Percentage	Chemical status (%)					
								C (%)	O (%)	P (%)	Mg (%)	Si (%)	K (%)
002	23.1	44.6	3.85	-	6,46	-	Atomic	56.25	24.15	4.37	0.70	0.67	3.69
100	25.1	46.1	-	2.02	-	21,7	mass	69.56	22.42	2.09	0.43	0.36	5.14

exhibited the highest ionic conductivity of $350.1 \text{ S cm}^2/\text{mol}$, supporting the performance of the BSF carbon electrode in the charge transfer process within supercapacitor devices. Based on this discussion, $1 \text{ M H}_2\text{SO}_4$ electrolyte solution proved to be the most suitable electrolyte type for supercapacitors utilizing activated carbon derived from banana stem fiber biomass.

The charging and discharging currents of the BSF- H_2SO_4 AC carbon electrode surpassed those of KOH and Na_2SO_4 electrolytes by 67%, producing a higher specific capacitance. In addition, employing a lower scan rate (1 mV/s) led to a greater specific capacitance output as seen in Figure 3(a–c). The relationship between the scan rate and the specific capacitance value (Figure 3d). Furthermore, the contribution capacitance was reviewed in detail via the Trensatti approach to confirm the self-doping effect of the O and P heteroatoms, as shown in Figure 3e. According to Figure 3e, BSF electrodes based on different electrolytes show a capacitance contribution dominated by EDLC capacitance of 68.91%, 54.21% and 73.05% for the precursors AC-BSF- H_2SO_4 , AC-BSF-KOH, and AC-BSF- Na_2SO_4 . Interestingly, the pseudocapacitance contribution of up to 45.79% reveals a redox reaction effect from the high N and O functional groups at the electrodes obtained.

The electrochemical properties of the AC-BSF electrode were further confirmed through the galvanostatic charge-discharge (GCD) method using the CD UR Red-ER 2018. This test involved the use of different types of electrolytes, namely acidic, basic, and neutral electrolytes (H_2SO_4 , KOH, and Na_2SO_4) at a concentration of 1 M . GCD measurements for each AC-BSF sample showed a distorted isosceles triangle-like curve shape, confirming the EDLC behavior of biomass materials as seen in Figure 4a. The AC-BSF- H_2SO_4 and AC-BSF-KOH electrodes, at a current density of 1 A ,

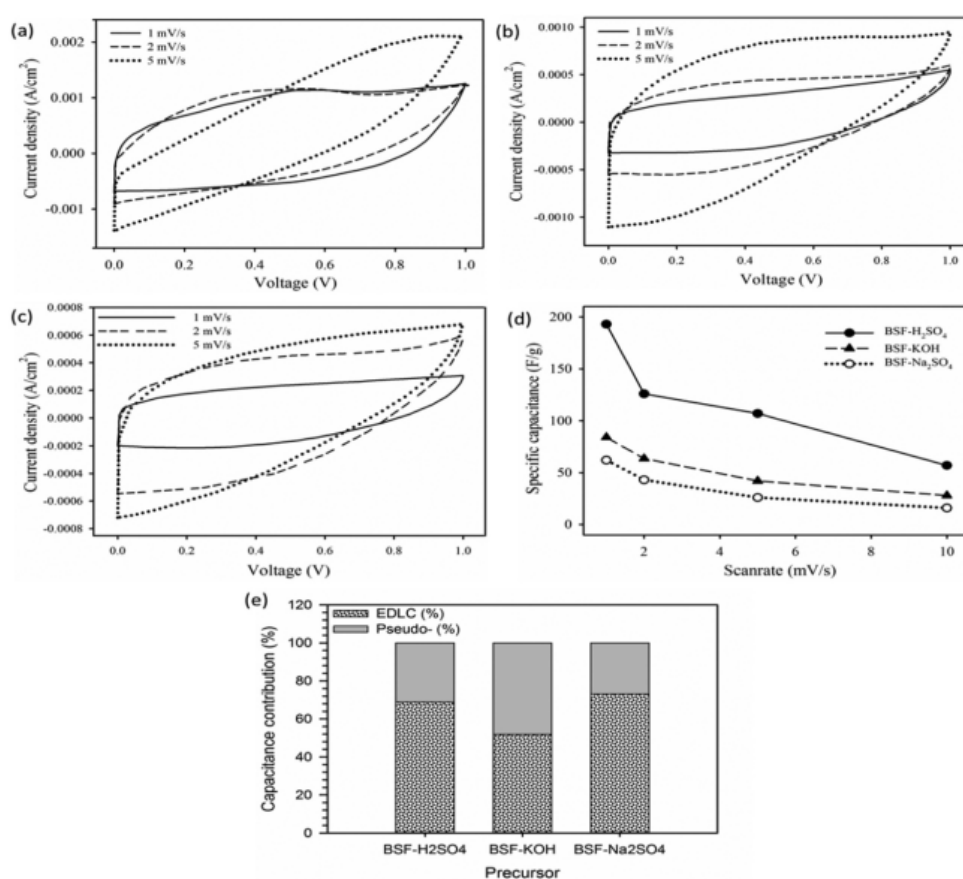


Figure 3. CV profile in aqueous electrolytes of (a) BSF- H_2SO_4 , (b) BSF-KOH, (c) BSF- Na_2SO_4 , (d) specific capacitance values for all electrolyte at scanrates (1, 2, and 5) mV/s, and (e) capacitance contribution of all precursor.

showed a slight curvature in the charging curve, confirming the presence of pseudocapacitance behavior due to the self-doping effect of dual heteroatoms O and P in Figure 4a, as described in the cyclic voltammetric analysis. GCD measurements at a current of 1 A confirmed the optimum performance of the AC-BSF- H_2SO_4 electrode, exhibiting the highest specific capacitance. This electrode demonstrated a maximum charge-discharge time and a low resistance, facilitating smooth ion diffusion into the electrode pores (Musyoka, Mutuma, and Manyala 2020).

Figure 4b showed the behavior of the BSF- H_2SO_4 AC electrode under various current densities (1, 2, and 5) A. The curve formed at 1 A current reflected the ideal electrochemical properties for a double-layer capacitor. It also described a very low resistance of 0.0093 Ω . Increasing the current to 2 A led to a smaller GCD curve with an increased resistance of 0.078 Ω . When the current is further increased to 5 A, the GCD curve was more narrowed, accompanied by an increased resistance of 0.179 Ω . The BSF-KOH AC electrode at 1 A current exhibited an ideal GCD profile for a double-layer electrochemical capacitor, with a slight bend indicating the influence of pseudocapacitance and a resistance of 0.085 Ω . On the other hand, the BSF- Na_2SO_4 AC electrode under current (1, 2, and 5) A displayed similar characteristics to the carbon electrode in H_2SO_4 and KOH electrolyte solutions, but with a higher resistance and no curvature in the charging curve, as seen in Figure 4d.

Further analysis was conducted on the electrochemical properties of the AC-BSF electrode using the GCD method to confirm the energy and power density of each electrolyte variation (Table 2). The AC-BSF- H_2SO_4 electrode exhibited optimal conditions with an energy density of 31.13 Wh/kg and the highest power density of 150.31 W/kg compared to AC-BSF-KOH and AC-BSF- Na_2SO_4 . In contrast, AC-KOH offered lower energy and power density values of 18.11 Wh/kg and 145.54 W/kg, respectively. AC-BSF- Na_2SO_4 only provided an energy and power density of 13.53 Wh/kg and 110 W/kg, respectively. Therefore, the H_2SO_4 electrolyte solution showed great potential and suitability as a charge carrier source in supercapacitor cell devices with BSF biomass-based electrode components, supporting superior supercapacitor performance (Taer et al. 2023). The electrochemical performance of the GCD method from the AC-BSF- H_2SO_4 electrode, including specific capacitance, energy density, and power density could compete with the results of previous studies.

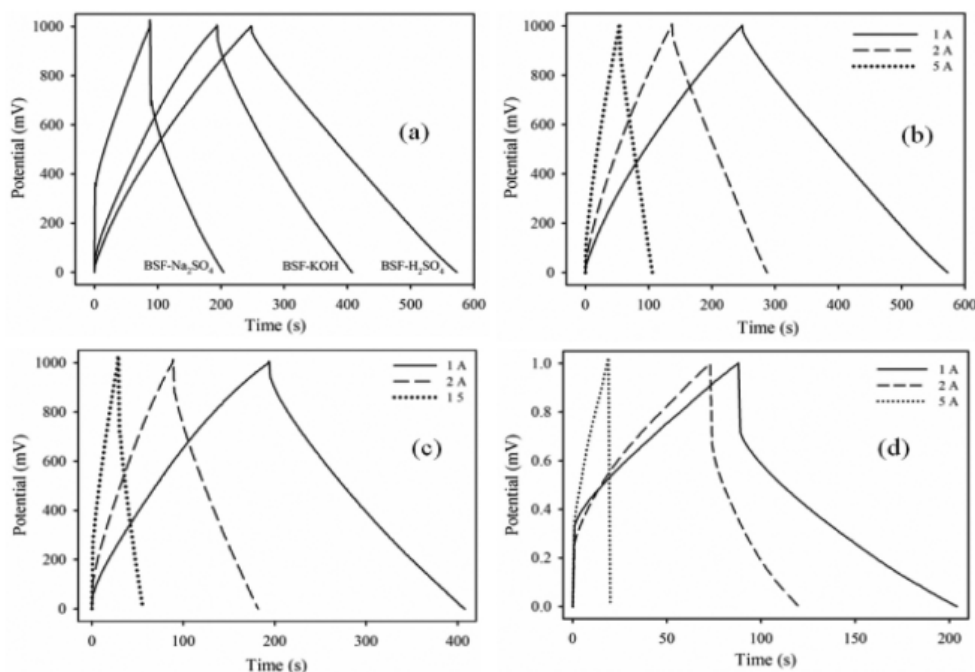


Figure 4. GCD curve (a) different electrolytes at 1 A, (b) BSF- H_2SO_4 , (c) BSF-KOH, (d) BSF- Na_2SO_4 at different current (1, 2, and 5 A).

Table 2. Electrochemical properties of different biomass-based carbon electrodes.

Samples	Electrolyte	C _{sp} (F/g)	Current (A/g)	E _{sp} (Wh/Kg)	P _{sp} (W/Kg)	Ref.
Banana leaves	6 M KOH	211	1	34.67	97.68	(Apriwandi et al. 2021)
Waste banana bract	1 M Na ₂ SO ₄	472	0.5	86	1280	(Priya, Kennedy, and Anand 2023)
Stinky bean seedpod	1 M KOH	193	0.5	10.58	720	(Malhotra, Valiollahi, and Wiinikka 2023)
Composite	6 M KOH	252	10	37.67	500	(Wang et al. 2023)
Syzygium Cumini Frutshell	6 M KOH	120	0.2	16.72	200	(Vinayagam et al. 2020)
AC-BSF	1 M H ₂ SO ₄	206.76	1	31.13	150.31	This research
	1 M KOH	132.57		18.11	145.54	
	1 M Na ₂ SO ₄	73.80		13.53	110	

Conclusion

In this work, AC-BSF nanosheets enriched with self-dual-doped O and P were successfully synthesized through the chemical activation of 0.5 M KOH via integrated pyrolysis (N₂-CO₂) at temperatures up to 850°C. The utilization of eco-friendly, cost-effective, and sustainable green electrode material derived from banana stem fiber exhibited remarkable electrochemical performance for supercapacitor applications. The synergistic effect of KOH/N₂-CO₂ at high temperatures produced a porous activated carbon material with amorphous porosity and high hydrophilicity and also increased the content of self-dual-doped heteroatoms O and P within the activated carbon material. This process involved redox reactions during electrochemical processes and led to the development of pseudocapacitance properties. The carbon purity reached 69.56%, with a surface area of 326.35 m²/g, and the optimal combination of micro-meso pores contributed positively to the ABSF electrode. Notably, the BSF AC electrode in 1 M H₂SO₄ aqueous electrolyte achieved a specific energy density and power of 31.13 Wh/kg and 150.31 W/kg, respectively. The synergistic combination of the mutually beneficial physical properties of the electrodes produced an extraordinary specific capacitance of 206.76 F/g. These results highlighted the potential of preparing AC nanosheets with high self-dual-doped O and P from banana stem fiber waste as promising electrodes for supercapacitors, enabling high-energy storage devices.

Acknowledgements

The research was financially supported by third years Project of Word Class Research (WCR) in [Kementerian Pendidikan, Kebudayaan, Riset, dan Teknologi, Republic of Indonesia](#) with the title "Supercapacitors with high energy and power density: Optimization of the electrode supply process" contract No.: 11312/UN19.5.1.3/AL.04/2023.

Disclosure statement

No potential conflict of interest was reported by the author(s).

Funding

The work was supported by the [Kementerian Pendidikan, Kebudayaan, Riset, dan Teknologi](#) [11312/UN19.5.1.3/AL.04/2023].

ORCID

Erman Taer <http://orcid.org/0000-0003-4463-8252>
 Novi Yanti <http://orcid.org/0000-0003-2892-9818>
 Apriwandi Apriwandi <http://orcid.org/0000-0003-3560-5571>
 Rika Taslim <http://orcid.org/0000-0003-1946-1299>

References

- 5 Açıklan, K. 2021. Determination of kinetic triplet, thermal degradation behaviour and thermodynamic properties for pyrolysis of a lignocellulosic biomass. *Bioresource Technology* 337 (May):125438. doi:10.1016/j.biortech.2021.125438.
- Apriwandi, A., E. Taer, R. Farma, R. N. Setiadi, and E. Amiruddin. 2021. A facile approach of micro-mesopores structure binder-free coin/monolith solid design activated carbon for electrode supercapacitor. *Journal of Energy Storage* 40 (June):102823. doi:10.1016/j.est.2021.102823.
- Awitdrus, A., D. A. Yusra, E. Taer, A. Agustino, A. Apriwandi, R. Farma, and R. Taslim. 2022. Biomass conversion into activated carbon as a sustainable energy material for the development of supercapacitor devices. *Energy Sources, Part A: Recovery, Utilization, & Environmental Effects* 44 (2):3349–59. doi:10.1080/15567011.2022.2064941.
- Chen, H., M. Li, C. Li, X. Li, Y. Wu, X. Chen, J. Wu, X. Li, and Y. Chen. 2022. Electrospun carbon nanofibers for lithium metal anodes: Progress and perspectives. *Chinese Chemical Letters* 33 (1):141–52. doi:10.1016/j.ccl.2021.08.097.
- Choi, H. Y., B. Lee, and Y. G. Jeong. 2023. Microstructures and electrochemical characterization of graphene oxide/carboxymethylated cellulose nanofibril-derived hybrid carbon aerogels for freestanding supercapacitor electrodes. *International Journal of Electrochemical Science* 18 (5):100101. doi:10.1016/j.ijoes.2023.100101.
- Dong, Y., W. Wang, W. Wang, D. Ma, S. Ma, C. Wang, D. Wang, and G. Shi. 2023. Synthesis of activated carbon nanofibers by bio-enzymatic method as electrode material for supercapacitors. *International Journal of Electrochemical Science* 18 (3):100024. doi:10.1016/j.ijoes.2023.01.002.
- Fang, H., D. Li, M. Zhao, Y. Zhang, J. Yang, and K. Wang. 2022. Research progress and prospect of hybrid supercapacitors as boosting the performance. *Energy Sources, Part A: Recovery, Utilization, & Environmental Effects* 1–18. doi:10.1080/15567036.2022.2033887.
- Farma, R., A. Putri, E. Taer, A. Awitdrus, and A. A. 2021. Synthesis of highly porous activated carbon nanofibers derived from bamboo waste materials for application in supercapacitor. *Journal of Materials Science: Materials in Electronics* 32 (6):7681–91. doi:10.1007/s10854-021-05420-3.
- Fu, H., X. Zhang, J. Fu, G. Shen, Y. Ding, Z. Chen, and H. Du. 2020. Single layers of MoS₂/Graphene nanosheets embedded in activated carbon nano fibers for high-performance supercapacitor. *Journal of Alloys and Compounds* 829:154557. doi:10.1016/j.jallcom.2020.154557.
- Kigozi, M., G. N. Kasozi, S. Balaso Mohite, S. Zamisa, R. Karpoomath, J. B. Kirabira, and E. Tebandeke. 2023. Non-emission hydrothermal low-temperature synthesis of carbon nanomaterials from poly (ethylene terephthalate) plastic waste for excellent supercapacitor applications. *Green Chemistry Letters and Reviews* 16 (1). doi: 10.1080/17518253.2023.2173025.
- Kumar, M., S. K. Shukla, S. N. Upadhyay, and P. K. Mishra. 2020. Analysis of thermal degradation of banana (Musa balbisiana) trunk biomass waste using iso-conversional models. *Bioresource Technology* 310 (April):123393. doi:10.1016/j.biortech.2020.123393.
- Lesbayev, B., M. Auyelkhanqyzy, G. Ustayeva, M. Yeleuov, N. Rakhymzhan, A. Maltay, and Y. Maral. 2023. Recent advances: Biomass-derived porous carbon materials. *South African Journal of Chemical Engineering* 43 (August 2022):327–36. doi:10.1016/j.sajce.2022.11.012.
- Liu, H., X. Huang, M. Zhou, M. Gu, M. Xu, L. Jiang, M. Zheng, S. Li, and Z. Miao. 2023. Efficient conversion of biomass waste to N/O co-doped hierarchical porous carbon for high performance supercapacitors. *Journal of Analytical and Applied Pyrolysis* 169 (August 2022):105844. doi:10.1016/j.jaap.2022.105844.
- Li, X., J. Zhang, B. Liu, and Z. Su. 2021. A critical review on the application and recent developments of post-modified biochar in supercapacitors. *Journal of Cleaner Production* 310: Elsevier Ltd. doi:10.1016/j.jclepro.2021.127428.
- Malhotra, J. S., R. Valiollahi, and H. Wiinikka. 2023. From wood to supercapacitor electrode material via fast pyrolysis. *Journal of Energy Storage* 57 (November 2022):106173. doi:10.1016/j.est.2022.106179.
- Mangiseti, S. R., M. Kamaraj, and R. Sundara. 2021. Large-scale single-step synthesis of wrinkled N-S doped 3D graphene like nanosheets from T₅₁er palm shoots for high energy density supercapacitors. *International Journal of Hydrogen Energy* 46 (1):403–15. doi:10.1016/j.ijhydene.2020.09.161.
- Misran, E., O. Bani, E. M. Situmeang, and A. S. Purba. 2022. Banana stem based activated carbon as a low-cost adsorbent for methylene blue removal: Isotherm, kinetics, and reusability. *Alexandria Engineering Journal* 61 (3):1946–55. doi:10.1016/j.aej.2021.07.022.
- Musyoka, N. M., B. K. Mutuma, and N. Manyala. 2020. Onion-derived activated carbons with enhanced surface area for improved hydrogen storage and electrochemical energy application. *RSC Advances* 10 (45):26928–36. doi:10.1039/D0RA04556J.
- 17 Priya, D. S., L. J. Kennedy, and G. T. Anand. 2023. Effective conversion of waste banana bract into porous carbon electrode for supercapacitor energy storage applications. *Results in Surfaces and Interfaces* 10 (August 2022):100096. doi:10.1016/j.rsufi.2023.100096.

- Shaku, B., T. P. Mofokeng, N. J. Coville, K. I. Ozoemena, and M. S. Maubane-Nkadimeng. 2023. Biomass valorisation of marula nutshell waste into nitrogen-doped activated carbon for use in high performance supercapacitors. *Electrochimica Acta* 442 (January):141828. doi:10.1016/j.electacta.2023.141828.
- Shang, Z., X. An, L. Liu, J. Yang, W. Zhang, H. Dai, H. Cao, Q. Xu, H. Liu, and Y. Ni. 2021. Chitin nanofibers as versatile bio-templates of zeolitic imidazolate frameworks for N-doped hierarchically porous carbon electrodes for supercapacitor. *Carbohydrate Polymers* 251 (29):117107. doi:10.1016/j.carbpol.2020.117107.
- Shanmuga Priya, M., P. Divya, and R. Rajalakshmi. 2020. A review status on characterization and electrochemical behaviour of biomass derived carbon materials for energy storage supercapacitors. *Sustainable Chemistry and Pharmacy* 16 (March):100243. doi:10.1016/j.scp.2020.100243.
- Taer, E., D. Afdal Yusra, A. Amri, T. R. Awitrus, A. Apriwandi, A. Putri, and A. Putri. 2020. The synthesis of activated carbon made from banana stem fibers as the supercapacitor electrodes. *Materials Today: Proceedings* 44:3346–49. doi:10.1016/j.matpr.2020.11.645.
- Taer, E., A. Apriwandi, S. Chow, and R. Taslim. 2023. Integrated pyrolysis approach of self-O-doped hierarchical porous carbon volumetric performance. *Diamond and Related Materials* 135:109866. doi:10.1016/j.diamond.2023.109866.
- Taer, E., A. Apriwandi, W. Windasari, R. Taslim, and M. Deraman. 2023. Novel laurel aromatic evergreen biomass derived hierarchical porous carbon nanosheet as sustainable electrode for high performance symmetric supercapacitor. *Journal of Energy Storage* 67:107567. doi:10.1016/j.est.2023.107567.
- Taer, E., N. Y. Effendi, R. Taslim, and A. Apriwandi. 2022. Interconnected micro-mesoporous carbon nanofiber derived from lemongrass for high symmetric supercapacitor performance. *Journal of Materials Research and Technology* 19:4721–32. doi:10.1016/j.jmrt.2022.06.167.
- Taer, E., N. Syamsunar, A. Apriwandi, and R. Taslim. 2023. Novel Solanum torvum fruit biomass-derived hierarchical porous carbon nanosphere as excellent electrode material for enhanced symmetric supercapacitor performance. *Jom*. doi:10.1007/s11837-023-05801-x.
- Taer, E., N. Yanti, J. A. Putri, A. Apriwandi, and R. Taslim. 2022 November. Novel macaroni-sponge-like pore structure biomass (*Zingiber officinale* Rosc. leaves)-based electrode material for excellent energy gravimetric supercapacitor. *Journal of Chemical Technology and Biotechnology* 98 (4):990–1002. doi:10.1002/jctb.7303.
- Vinayagam, M., R. Suresh Babu, A. Sivasamy, and A. L. Ferreira de Barros. 2020. Biomass-derived porous activated carbon from *Syzygium cumini* fruit shells and *Chrysopogon zizanioides* roots for high-energy density symmetric supercapacitors. *Biomass and Bioenergy* 143 (October):105838. doi:10.1016/j.biombioe.2020.105838.
- Wang, Y., Y. Lu, Z. Hu, J. Sun, G. Xiao, H. Zhao, J. Zhu, and Z. Liu. 2023. Electrochemistry communications facile preparation of Zr @ carbon electrodes based on polyimide/Uio-66 composites for supercapacitors. *Electrochemistry Communications* 148 (February):107449. doi:10.1016/j.elecom.2023.107449.
- Wang, H., H. Niu, H. Wang, W. Wang, X. Jin, H. Wang, H. Zhou, and T. Lin. 2021. Micro-meso porous structured carbon nanofibers with ultra-high surface area and large supercapacitor electrode capacitance. *Journal of Power Sources* 482 (September 2020):228986. doi:10.1016/j.jpowsour.2020.228986.
- Wang, W., D. Yang, Z. Huang, H. Hu, L. Wang, and K. Wang. 2022. Electrodeless nanogenerator for dust recover. *Energy Technology* 10 (12):2200699. doi:10.1002/ente.202200699.
- Xuan, X., M. Wang, W. You, S. Manickam, Y. Tao, J. Y. Yoon, and X. Sun. 2023. Hydrodynamic cavitation-assisted preparation of porous carbon from garlic peels for supercapacitors. *Ultrasonics Sonochemistry* 94 (December 2022):106333. doi:10.1016/j.ulsonch.2023.106333.
- Yaglikci, S., Y. Gokce, E. Yagmur, and Z. Aktas. 2020. The performance of sulphur doped activated carbon supercapacitors prepared from waste tea. *Environmental Technology (United Kingdom)* 41 (1):36–48. doi:10.1080/09593330.2019.1575480.
- Yang, X., Y. Zheng, C. He, Y. Qiu, W. Hou, B. Lu, Y. Chen, B. Huang, J. Lv, and G. Lin. 2023. Preparation of biomass-based N, P, and S co-doped porous carbon with high mesoporosity based on the synergistic effect of NaOH/thiourea and melamine phosphate and its application in high performance supercapacitors. *Journal of Analytical and Applied Pyrolysis* 169 (July 2022):105822. doi:10.1016/j.jaap.2022.105822.
- Yan, C., S. Jia, J. Wei, J. Guan, and Z. Shao. 2023. Efficient dual conductive network based on layered double hydroxide nanospheres and nanosheets anchored in N-carbon nanofibers for asymmetric supercapacitors. *Journal of Alloys and Compounds* 930:167332. doi:10.1016/j.jallcom.2022.167332.
- Ye, R., J. Cai, Y. Pan, X. Qiao, and W. Sun. 2020. Microporous carbon from malva nut for supercapacitors: Effects of primary carbonizations on structures and performances. *Diamond and Related Materials* 105 (December 2019). doi:10.1016/j.diamond.2020.107816.
- Yetri, Y., A. T. Hoang, M. Mursida, D. Dahlan, M. Muldarisnur, E. Taer, and M. Q. Chau (2020). Synthesis of activated carbon monolith derived from cocoa pods for supercapacitor electrodes application. *Energy Sources, Part A: Recovery, Utilization and Environmental Effects*, 1–15. doi: 10.1080/15567036.2020.1811433
- Zhang, M., W. Wang, G. Xia, L. Wang, and K. Wang. 2023. Self-powered electronic skin for remote human-machine synchronization. *ACS Applied Electronic Materials* 5 (1):498–508. doi:10.1021/acsaelm.2c01476.

- Zhang, C., B. Yuan, Y. Liang, L. Yang, L. Bai, H. Yang, D. Wei, F. Wang, Q. Wang, W. Wang, et al. 2021. Carbon nanofibers enhanced solar steam generation device based on loofah biomass for water purification. *Materials Chemistry and Physics* 248 (October 2020):123998. doi:10.1016/j.matchemphys.2020.123998.
- Zhou, Q., and H. Yao. 2022. Recent development of carbon electrode materials for electrochemical supercapacitors. *Energy Reports* 8:656–61. doi:10.1016/j.egy.2022.09.167.

ORIGINALITY REPORT

12%

SIMILARITY INDEX

8%

INTERNET SOURCES

9%

PUBLICATIONS

4%

STUDENT PAPERS

PRIMARY SOURCES

- 1 Hyeong Yeol Choi, Byoung-Min Lee, Young Gyu Jeong. "Microstructures and electrochemical characterization of graphene oxide/carboxymethylated cellulose nanofibril-derived hybrid carbon aerogels for freestanding supercapacitor electrodes", International Journal of Electrochemical Science, 2023
Publication
- 2 people.busitema.ac.ug
Internet Source
- 3 physics.iitm.ac.in
Internet Source
- 4 qmro.qmul.ac.uk
Internet Source
- 5 Ahmad Nawaz, Pradeep Kumar. "Optimization of process parameters of Lagerstroemia speciosa seed hull pyrolysis using a combined approach of Response Surface Methodology (RSM) and Artificial Neural Network (ANN) for renewable fuel production", Bioresource Technology Reports, 2022

6	Ayman F. Abou-Hadid, Usama A. El-Behairy, Mahmoud M. Elmalih, Enas Amdeha et al. "Production of efficient carbon fiber from different solid waste residuals for adsorption of hazardous metals from wastewater samples", Biomass Conversion and Biorefinery, 2022 Publication	<1 %
7	Submitted to Monash University Student Paper	<1 %
8	www.ascidatabase.com Internet Source	<1 %
9	www.ijche.com Internet Source	<1 %
10	Anindita Hazarika, Meera Yadav. "Biomineralization of carbon dioxide by carbonic anhydrase", Biocatalysis and Agricultural Biotechnology, 2023 Publication	<1 %
11	P. Divya, Nunna Guru Prakash, Tae Jo Ko, P. Rosaiah. "Metal/Metal Oxide (N-MnO/rGO) Encapsulated Carbon Nanofiber Composites for High-performance Li-ion Batteries", Journal of Cluster Science, 2022 Publication	<1 %
12	Submitted to University of Massachusetts, Lowell Student Paper	<1 %

13

Michal Bláha, Václav Valeš, Zdeněk Bastl, Martin Kalbáč, Hidetsugu Shiozawa. "Host-Guest Interactions in Metal-Organic Frameworks Doped with Acceptor Molecules as Revealed by Resonance Raman Spectroscopy", *The Journal of Physical Chemistry C*, 2020

Publication

<1 %

14

raccefyn.co

Internet Source

<1 %

15

Fatemeh Maghsoodi Goushki, Mohammad Reza Islami, Vajihe Nejadshafiee.

"Preparation of eco-friendly nanocomposites based on immobilization of magnetic activated carbon with tartaric acid: Application for adsorption of heavy metals and evaluation of their catalytic activity in C-C coupling reaction", *Materials Science and Engineering: B*, 2022

Publication

<1 %

16

Submitted to The University of Manchester

Student Paper

<1 %

17

Md Sumon Reza, Shammya Afroze, Kairat Kuterbekov, Asset Kabyshev et al.

"Advanced Applications of Carbonaceous Materials in Sustainable Water Treatment, Energy Storage, and CO₂ Capture: A Comprehensive Review", *Sustainability*, 2023

Publication

<1 %

18

Mohd Zahid Ansari, Dip K. Nandi, Petr Janicek, Sajid Ali Ansari, Rahul Ramesh, Taehoon Cheon, Bonggeun Shong, Soo-Hyun Kim. "Low-Temperature Atomic Layer Deposition of Highly Conformal Tin Nitride Thin Films for Energy Storage Devices", ACS Applied Materials & Interfaces, 2019

Publication

<1 %

19

Submitted to University of Lincoln

Student Paper

<1 %

20

Submitted to Hawaii Preparatory Academy

Student Paper

<1 %

21

Liping Chen, Xiaobo Wu, António M. Lopes, Xin Li, Penghua Li, Ranchao Wu. "State of charge estimation for lithium-ion batteries based on a novel complex-order model", Communications in Nonlinear Science and Numerical Simulation, 2023

Publication

<1 %

22

Khabibulla A. Abdullin, Maratbek T. Gabdullin, Zhanar K. Kalkozova, Shyryn T. Nurbolat, Mojtaba Mirzaeian. "Efficient Recovery Annealing of the Pseudocapacitive Electrode with a High Loading of Cobalt Oxide Nanoparticles for Hybrid Supercapacitor Applications", Nanomaterials, 2022

Publication

<1 %

- | | | |
|----|---|------|
| 23 | Natália Gabriele Camparotto, Gustavo Rocha Paixão, Giani de Vargas Brião, Rafael L. Oliveira et al. "Comparative effect of mesoporous carbon doping on the adsorption of pharmaceutical drugs in water: Theoretical calculations and mechanism study", Environmental Toxicology and Pharmacology, 2023
Publication | <1 % |
| 24 | Submitted to University of Reading
Student Paper | <1 % |
| 25 | dro.deakin.edu.au
Internet Source | <1 % |
| 26 | watermark.silverchair.com
Internet Source | <1 % |
| 27 | Submitted to Hellenic Open University
Student Paper | <1 % |
| 28 | journal.upgris.ac.id
Internet Source | <1 % |
| 29 | Bingyi Li, Xiaolu Wang, Zhidong Xia, Wei Zhou, Yufeng Wu, Guangze Zhu. "Co-pyrolysis of waste polyester enameled wires and polyvinyl chloride: Evolved products and pyrolysis mechanism analysis", Journal of Analytical and Applied Pyrolysis, 2023
Publication | <1 % |
| 30 | Hongkang Wang, Xuming Yang, Qizhen Wu, Qiaobao Zhang et al. "Encapsulating | <1 % |

Silica/Antimony into Porous Electrospun Carbon Nanofibers with Robust Structure Stability for High-Efficiency Lithium Storage", ACS Nano, 2018

Publication

31

S. Shivakumara, N. Munichandraiah. "Asymmetric supercapacitor based on nanostructured porous manganese oxide and reduced graphene oxide in aqueous neutral electrolyte", Solid State Communications, 2017

Publication

<1 %

32

rcastoragev2.blob.core.windows.net
Internet Source

<1 %

33

repository.unri.ac.id
Internet Source

<1 %

34

Xin Su, Dezhao Hao, Mingyue Sun, Tingshu Wei, Dake Xu, Xicheng Ai, Xinglin Guo, Tong Zhao, Lei Jiang. "Nature Sunflower Stalk Pith with Zwitterionic Hydrogel Coating for Highly Efficient and Sustainable Solar Evaporation", Advanced Functional Materials, 2021

Publication

<1 %

35

insightsociety.org
Internet Source

<1 %

36

orbit.dtu.dk
Internet Source

<1 %

37

Internet Source

<1 %

38

Jiaxin Zhang, Zhilin Yu, Yunqin Li, Xueqiang Wang. "Uncovering Bias in Objective Mapping and Subjective Perception of Urban Building Functionality: A Machine Learning Approach to Urban Spatial Perception", Land, 2023

Publication

<1 %

39

anhuilu.dlut.edu.cn

Internet Source

<1 %

40

pcmp.springeropen.com

Internet Source

<1 %

41

Zhenbao Feng, Wei Ding, Yangming Lin, Feng Guo, Xiaoyan Zhang, Tengshuo Song, Hengshuai Li, Cailong Liu. "Electron momentum density of boron-doped carbon nano-onions studied by electron energy-loss spectroscopy", Physical Chemistry Chemical Physics, 2021

Publication

<1 %

42

hdl.handle.net

Internet Source

<1 %

43

Bong Gill Choi, MinHo Yang, Won Hi Hong, Jang Wook Choi, Yun Suk Huh. "3D Macroporous Graphene Frameworks for Supercapacitors with High Energy and Power Densities", ACS Nano, 2012

Publication

<1 %

44	www.sustainablelivingdirectory.com Internet Source	<1 %
45	Chao Gao, Lijun Huang, Yuhui Feng, Erya Gao, Zhongqing Yang, Kai Wang. "Thermal field modeling and characteristic analysis based on oil immersed transformer", Frontiers in Energy Research, 2023 Publication	<1 %
46	html.rhhz.net Internet Source	<1 %
47	Ali Izadi-Najafabadi, Satoshi Yasuda, Kazufumi Kobashi, Takeo Yamada et al. "Extracting the Full Potential of Single-Walled Carbon Nanotubes as Durable Supercapacitor Electrodes Operable at 4 V with High Power and Energy Density", Advanced Materials, 2010 Publication	<1 %
48	jurnal.amikwidyialoka.ac.id Internet Source	<1 %
49	medworm.com Internet Source	<1 %
50	nlist.inflibnet.ac.in Internet Source	<1 %
51	publications.iitm.ac.in Internet Source	<1 %
52	www.aimspress.com Internet Source	<1 %

53 www.chinchemlett.com.cn <1 %
Internet Source

54 www.oepm.es <1 %
Internet Source

55 www.unboundmedicine.com <1 %
Internet Source

56 Aoife C. Power, Brian Gorey, Shaneel Chandra, James Chapman. "Carbon nanomaterials and their application to electrochemical sensors: a review", *Nanotechnology Reviews*, 2018
Publication

57 Ming Zhang, Wanli Wang, Guoting Xia, Licheng Wang, Kai Wang. "Self-Powered Electronic Skin for Remote Human–Machine Synchronization", *ACS Applied Electronic Materials*, 2023
Publication

Exclude quotes Off

Exclude matches Off

Exclude bibliography Off